Structural insights into the catalytic mechanism of lovastatin hydrolase

Received for publication, November 15, 2019, and in revised form, December 7, 2019 Published, Papers in Press, December 15, 2019, DOI 10.1074/jbc.RA119.011936

Yajing Liang[‡§] and Xuefeng Lu[‡§¶1]

From the [‡]Key Laboratory of Biofuels and [§]Shandong Provincial Key Laboratory of Synthetic Biology, Qingdao Institute of Bioenergy and Bioprocess Technology, Chinese Academy of Sciences, Qingdao 266101, China and the [¶]Laboratory for Marine Biology and Biotechnology, Qingdao National Laboratory for Marine Science and Technology, Qingdao 266003, China

Edited by Joseph M. Jez

The lovastatin hydrolase PcEST from the fungus *Penicillium chrysogenum* exhibits enormous potential for industrial-scale applications in single-step production of monacolin J, the key precursor for synthesis of the cholesterol-lowering drug simvastatin. This enzyme specifically and efficiently catalyzes the conversion of lovastatin to monacolin J but cannot hydrolyze simvastatin. Understanding the catalytic mechanism and the structure–function relationship of PcEST is therefore important for further lovastatin hydrolase screening, engineering, and commercial applications. Here, we solved four X-ray crystal structures, including apo PcEST (2.3 Å), PcEST in complex with monacolin J (2.48 Å), PcEST complexed with the substrate analog simvastatin (2.4 Å), and an inactivated PcEST variant (S57A) with the lovastatin substrate (2.3 Å). Structure-based biochemical analyses and mutagenesis assays revealed that the Ser^{57} (nucleophile)–Tyr^{170} (general base)–Lys^{60} (general acid) catalytic triad, the hydrogen-bond network (Trp^{344} and Tyr^{127}) around the active site, and the specific substrate-binding tunnel together determine efficient and specific lovastatin hydrolysis by PcEST. Moreover, steric effects on nucleophilic attack caused by the 2′,2-dimethybutyryl group of simvastatin resulted in no activity of PcEST on simvastatin. On the basis of structural comparisons, we propose several indicators to define lovastatin esterases. Furthermore, using structure-guided enzyme engineering, we developed a PcEST variant, D106A, having improved solubility and thermostability, suggesting a promising application of this variant in industrial processes. To our knowledge, this is the first report describing the mechanism and structure–function relationship of lovastatin hydrolase and providing insights that may guide rapid screening and engineering of additional lovastatin esterase variants.

This work was supported by National Natural Science Foundation of China Grant 31700051 (to Y. L.), Natural Science Foundation of Shandong Province Grant ZR2017BC065 (to Y. L.), Science and Technology Service Network Initiative of the Chinese Academy of Sciences Grant KFJ-STS-ZDTP-031, and a Shandong Taishan Scholarship (to X. L.). The authors declare that they have no conflicts of interest with the contents of this article.

This article contains Tables S1 and S2 and Figs. S1–S3.

The atomic coordinates and structure factors (codes 6KJC, 6KJE, 6KJF, and 6KJD) have been deposited in the Protein Data Bank (http://wwpdb.org/).

[1] To whom correspondence should be addressed: Qingdao Institute of Bioenergy and Bioprocess Technology, Chinese Academy of Sciences, 189 Songling Rd., Qingdao 266101, China. Tel.: 86-532-80662712; E-mail: lvxf@qibebt.ac.cn.

Simvastatin, a derivative of the fungal polyketide lovastatin, is a major drug used to treat hypercholesterolemia. It is industrially produced through three steps: 1) *Aspergillus terreus* fermentation to produce lovastatin; 2) lovastatin alkaline hydrolysis to monacolin J; and 3) chemical or biological transformation of monacolin J to produce simvastatin (Fig. 1) (1–5). After the above steps, the 2-methylbutyryl side chain of lovastatin will be replaced by the 2,2-dimethylbutyryl side chain, thereby producing simvastatin. However, the multistep alkaline hydrolysis process to produce monacolin J is complicated, expensive, and environmentally unfriendly. Enzymatic synthesis using a specific lovastatin hydrolase is one of the alternative methods for the green production of monacolin J. In addition to their important role in green processes, specific lovastatin hydrolases without simvastatin hydrolysis activity are also industrially important because of their use in removing the residual lovastatin in simvastatin samples.

The discovery of lovastatin hydrolases with industrial application potential has been very slow. As early as 1997, a specific lovastatin esterase (unpublished protein sequence) was isolated and purified by Merck (6). Subsequently, this strain was used to establish a fermentative conversion system for monacolin J production (7). In 2004, Morgan reported another specific lovastatin esterase, EcBla4 (8). However, K_m values of up to 200–300 μM lovastatin restrict the industrial use of these lovastatin esterases to produce monacolin J. In 2017, we reported that a specific lovastatin esterase from *Penicillium chrysogenum* (called PcEST) catalyzed the single-step conversion of lovastatin to monacolin J with a 232-fold higher catalytic efficiency than EcBla4 (Table 1) and simultaneously displayed no activity against simvastatin. Further, we achieved ~95% conversion by heterologously expressing PcEST in an industrial *A. terreus* strain (2). Recently, we further reduced the lovastatin residual using a directed evolutionary PcEST mutant, Q140L, which presents 2.2-fold improved solubility, 1-fold enhanced catalytic efficiency, and 3 °C increased $T_{50}{}^{10}$ over the purified WT PcEST (9). All of these results clearly suggest the huge industrial application potential of PcEST.

Bioinformatics analyses showed that the function-identified proteins with the top three sequence identities (~36–40%) with PcEST are LovD from *A. terreus*, mokF from *Monascus pilosus*, and mlcH from *Penicillium citrinum* (Fig. S1). Interestingly, all of them are acyltransferases, which are mainly responsible for the transacylation reaction in different statin biosyn-

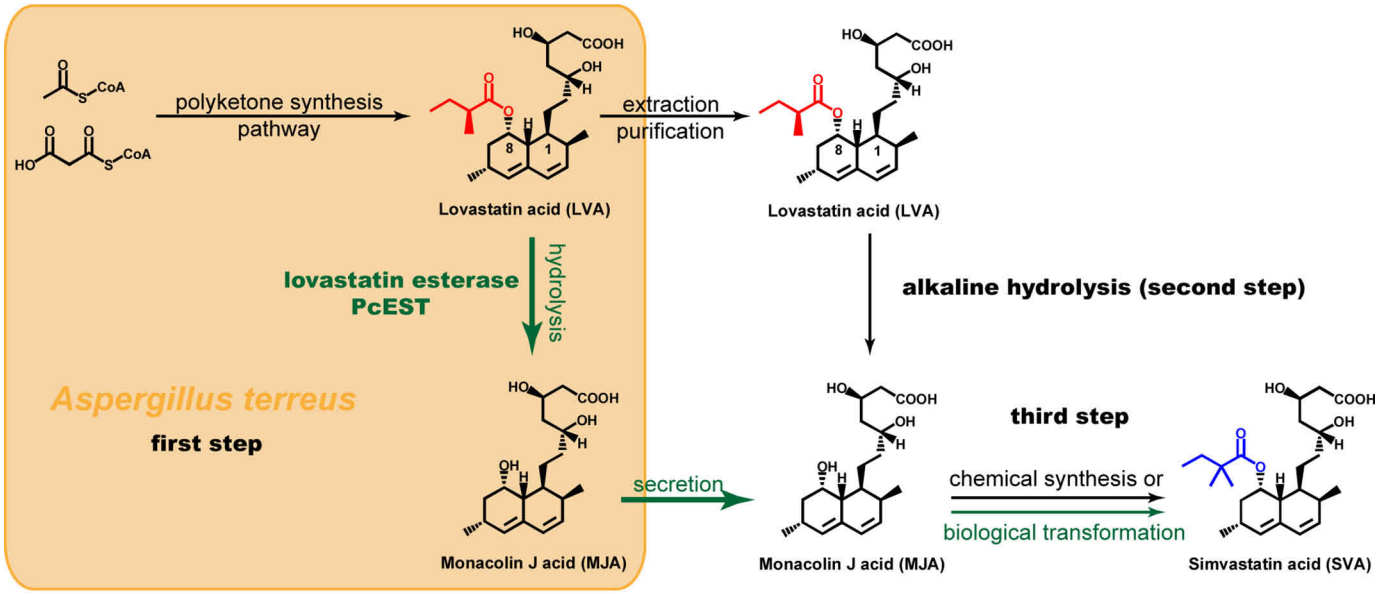

Figure 1. The industrial process for simvastatin production (2). Simvastatin only has one more methyl group than lovastatin. The 2-methylbutyryl side chain of lovastatin and 2′2-dimethybutyryloxy side chain of simvastatin are colored *red* and *blue*, respectively. The biological transformation route of simvastatin is labeled by a *green arrow*.

Table 1

Kinetic analysis with lovastatin of PcEST and its mutants

The values shown represent the averages of at least two repetitive measurements plus standard deviation.

Enzyme	K_m	k_{cat}	k_{cat}/K_m	Reference
	μM	min^{-1}	$min^{-1}\ \mu M^{-1}$	
PcEST	39.4 ± 4.3	194.6 ± 5.5	4.9 ± 0.4	Huang *et al.* (2) (37°)
EcBla4	237.5 ± 15.5	5.0 ± 0.1	0.0211 ± 0.0009	
LovD	560 ± 50	0.21 ± 0.01	0.0004 ± 0.000016	Xie *et al.* (10) (25°)
PcEST	5.46 ± 0.67	204.1 ± 5.93	37.38 ± 3.50	This work (30°)
Y127F	218 ± 23.15	8.93 ± 0.35	0.04 ± 0.003	
W344F	151.4 ± 28.69	1.26 ± 0.08	0.008 ± 0.0010	
D106A	8.67 ± 2.06	175.8 ± 8.99	20.28 ± 3.78	
D131A	9.11 ± 2.09	158.7 ± 9.0	17.42 ± 3.01	

thetic pathways. LovD is a well-studied enzyme with the highest sequence identity (up to 40%) with PcEST. This enzyme mainly catalyzes the transfer of the 2-methylbutyl side chain to monacolin J for the synthesis of lovastatin. In addition to acyltransferase activity, LovD also reversely catalyzes the lovastatin hydrolysis reaction with k_{cat} and K_m values of 0.21 ± 0.01 min^{-1} and 0.56 ± 0.05 mM, respectively (10), which represents an ~10^{-5}-fold catalytic efficiency of PcEST (Table 1). However, the specific lovastatin esterase EcBla4 shares only 16.8% sequence identity with PcEST. Moreover, all of these enzymes contain the conserved S*XX*K motif (where *X* represents any residue), which is important for catalysis in many serine-based enzymes (11). These results mean that screening for new and efficient lovastatin hydrolases through homologous sequence alignment methods is relatively inefficient and uneconomical. However, to date, the specific catalytic mechanism and structure–function relationships of lovastatin hydrolase have not been reported. Thus, it is important to clarify the specific and efficient lovastatin hydrolysis mechanism of PcEST to enable further rapid screening, protein engineering, and commercial application of lovastatin esterases.

In the present study, we solved four crystal structures of the lovastatin hydrolase PcEST, including apo PcEST, PcEST in complex with monacolin J, PcEST in complex with simvastatin, and the S57A inactivation mutant with the substrate lovastatin. Structure-based biochemical analyses and mutagenesis assays revealed the efficient and specific lovastatin hydrolysis mechanism and identified why PcEST has no activity toward simvastatin. In addition, based on structural comparisons, several indicators were proposed for the screening of subsequent lovastatin esterases. Furthermore, we successfully developed a solubility and thermostability improved D106A mutant through structure-guided enzyme engineering, suggesting a promising application of this variant in industrial processes.

Results and discussion

Sequence analysis of PcEST

First, the sequence alignment of 15 enzymes including PcEST, EcBla4, and members of the carboxylesterases family, acyltransferase family, and β-lactamase family was performed (Fig. S1). Although PcEST shares only 16.8% sequence identity with EcBla4, both enzymes contain the conserved S*XX*K motif of β-lactamases or family VIII carboxylesterases. In this motif, the serine acts as a nucleophile and initiates hydrolysis (12). In addition to the S*XX*K motif, PcEST has two motifs characteristic of family VIII carboxylesterases, Y*XX* and WGG (absent in EcBla4) (11). However, the highly conserved Y*X*N and K(T/S)G

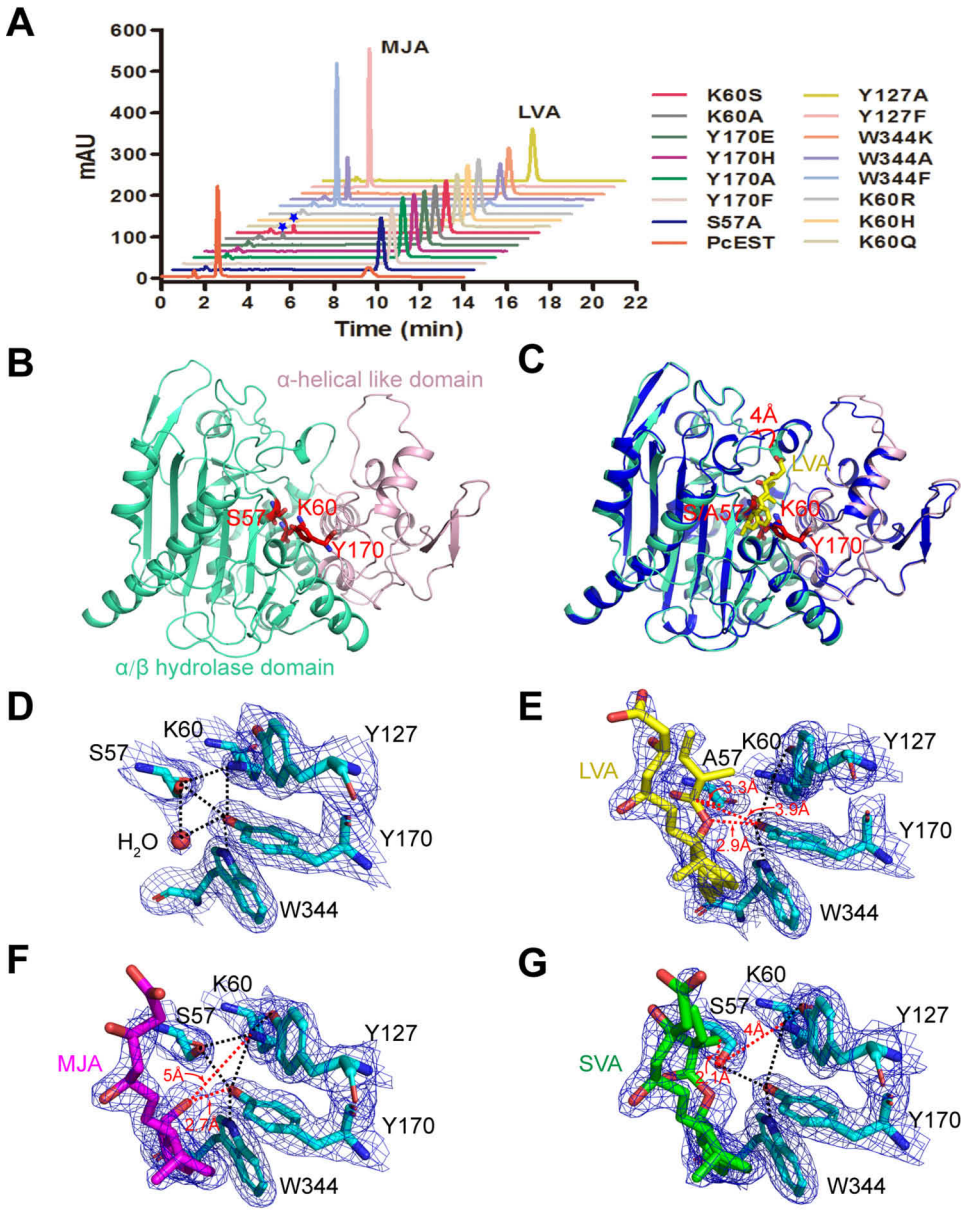

Figure 2. Mutagenesis and structural analyses of PcEST. *A*, lovastatin hydrolysis activity of PcEST mutants *in vitro*. The final concentration of all mutants is 100-fold greater than the WT PcEST control. The substrate lovastatin acid is abbreviated as *LVA*, and the product monacolin J acid is abbreviated as *MJA*. Moreover, the monacolin J acid peaks in mutants K60S and K60A HPLC curves are marked by *asterisks*. *B*, cartoon representation of the apo PcEST structure. Two domains are colored separately in *lime green* and *light pink*. The possible Ser^{57}–Lys^{60}–Tyr^{170} catalytic triad is shown as *sticks* with *red*. *C*, superimposition of the apo PcEST structure and S57A–lovastatin complex. S57A is presented with *blue*, and lovastatin is shown with *yellow sticks*. The conformational change in PcEST loop 238–245 after statin binding is marked with a *red arrow*. *D–G*, zoomed view of the apo PcEST and three PcEST–ligand complex catalytic centers. The $2F_o - F_c$ densities for the active site are contoured in *blue* at 1.5 σ. Hydrogen bonds are indicated by *black dashed lines*, and H_2O is shown as a *red ball*. The distances between key atoms that do not form hydrogen bonds are labeled in *red*.

motifs found in β-lactamases are not present in PcEST (13). These sequence analyses imply that PcEST is a family VIII carboxylesterase, with Ser^{57} as a putative nucleophile. Elimination of Ser^{57} nucleophilic activity in the S57A mutant completely abolished lovastatin hydrolysis, supporting the key role of Ser^{57} in PcEST-mediated lovastatin hydrolysis (Fig. 2*A*).

Overall structure of PcEST

To gain deeper insights into the structure–function relationships of PcEST, four crystal structures, including apo PcEST, PcEST–monacolin J complex, PcEST-simvastatin complex, and the S57A inactivation mutant with the substrate lovastatin complex, were solved. The structure resolutions of apo PcEST, S57A–lovastatin complex, PcEST–monacolin J complex, and PcEST–simvastatin complex are 2.3, 2.3, 2.48, and 2.4 Å, respectively. The data collection and refinement statistics are provided in Table S2.

Like other reported family VIII esterases (11, 14, 15), the PcEST proteins in all four structures adopt a two-domain modular structure containing a typical α/β hydrolase domain (residues 1–75 and 189–399) and a small α-helical like domain (residues 76–188). A highly hydrophobic substrate-binding pocket is formed at the two-domain interface with the con-

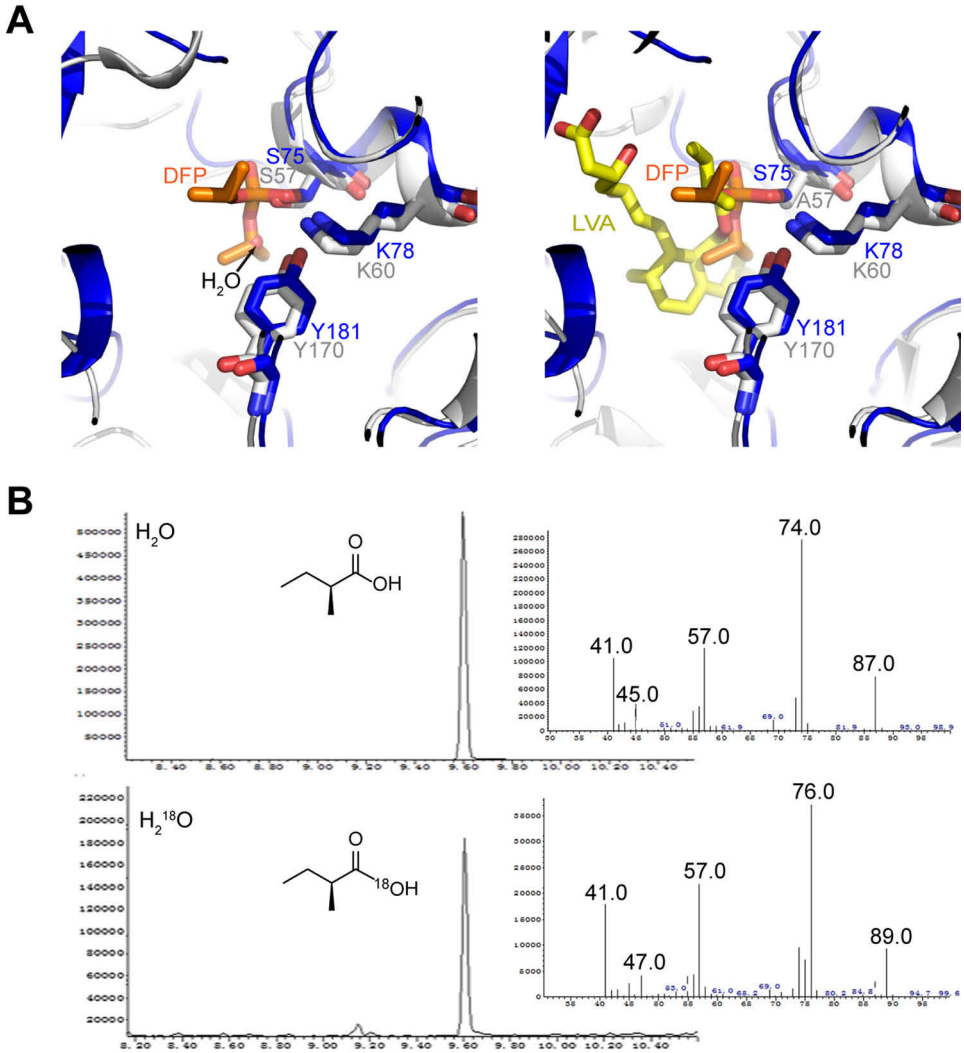

Figure 3. Verification of two nucleophiles in PcEST-mediated lovastatin hydrolysis. *A*, active site superimposition of the apo PcEST (*left panel*) or S57A–LVA complex (*right panel*) and the DFP-bound esterase EstB. PcEST or S57A and EstB are separately colored *white* and *blue*. The catalytic triads are shown as *sticks*, and H_2O in apo PcEST is shown as a *red ball*. DFP (*orange*) overlaps with the 2-methylbutyryl side chain of lovastatin (*yellow*) and the possible catalytic H_2O in PcEST. *B*, $H_2{}^{18}O$ isotope labeling assay using GC-MS detection.

served ^{57}SATK^{60} motif in the floor of the interface depression (Fig. 2, *B* and *C*).

Possible catalytic mechanism in PcEST-mediated lovastatin hydrolysis

We then examined the PcEST-mediated lovastatin hydrolysis mechanism. The general mechanism of family VIII esterases is thought to occur via two successive nucleophilic attacks by the serine in the Ser–Lys–Tyr catalytic triad and a water molecule (11). In fact, this mechanism is proposed with reference to the mechanism of class C β-lactamases because of the high structural similarity between the two. However, there is a lack of sufficient experiments to verify this mechanism. Although the nucleophile of serine in the catalytic triad is highly definitive, which residue(s) actually activates the serine and the second nucleophile of H_2O to initiate deacylation are matters of debate because of insufficient evidence.

In PcEST, the putative nucleophilic Ser^{57} is indeed neighboring the carbonyl carbon in the 2-methylbutyryl group of lovastatin, satisfying the requirement of a nucleophilic reaction. Further, Ser^{57} forms hydrogen bonds with Lys^{60} and Tyr^{170}, completing the PcEST catalytic triad (Fig. 2, *D* and *E*). Moreover, this putative Ser^{57}–Lys^{60}–Tyr^{170} catalytic triad completely overlaps the Ser^{75}–Lys^{78}–Tyr^{181} catalytic triad of esterase EstB (PDB[2] code 1CI9) (11), suggesting these residues indeed comprise the catalytic site (Fig. 3*A*). Furthermore, the phosphoryl group of the diisopropyl-fluorophosphate (DFP, an inhibitor of serine hydrolases using its phosphoryl group covalent attachment to catalytic serine) in the EstB structure matches well with the carbonyl group of lovastatin (Fig. 3*A*). These structural analyses, combined with abolished S57A activity, demonstrate the nucleophilic function of Ser^{57}.

Additionally, both Lys^{60} and Tyr^{170} are able to deprotonate Ser^{57}, indicating their potential as general bases. However, providing a proton to the leaving group by a general base is also necessary for completing the catalytic reaction. Thus, the distance between the C8 hydroxyl group in monacolin J and Tyr^{170}

[2] The abbreviations used are: PDB, Protein Data Bank; DFP, diisopropyl-fluorophosphate; ITC, isothermal titration calorimetry.

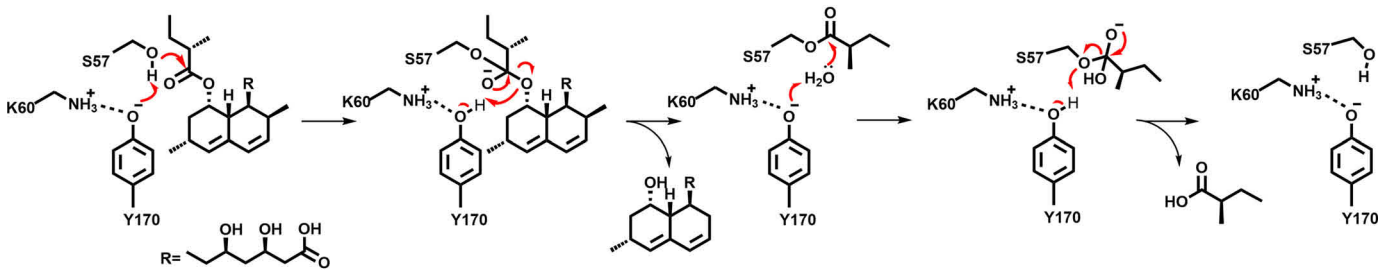

Figure 4. Proposed catalytic mechanism of PcEST-mediated lovastatin hydrolysis. Two successive nucleophilic reactions initiated by the Ser^{57} residue in the Ser^{57}–Tyr^{170} (general base)–Lys^{60} (general acid) catalytic triad and a water molecule achieve efficient lovastatin hydrolysis to produce monacolin J and 2-methylbutyric acid.

(2.7 Å) or Lys^{60} (5 Å) determines the possibility of Tyr^{170} as a general base, but not Lys^{60}, in PcEST-mediated lovastatin hydrolysis (Fig. 2*F*). To further confirm this hypothesis, a series of Tyr^{170} or Lys^{60} mutants was used to assay lovastatin hydrolase activity (Fig. 2*A*). All Tyr^{170} mutants lost lovastatin hydrolase activity. However, only Lys^{60} mutants with long-side-chain substitution had abolished activity. These results indicate that the Tyr^{170} phenolic hydroxyl group is an essential general base, with Lys^{60} acting as a general acid aiding the position and polarization of Tyr^{170}.

In terms of the deacylation mechanism, an H_2O molecule forms hydrogen bonds with both Ser^{57} and Tyr^{170} in apo PcEST and is replaced by lovastatin upon substrate binding, making it an ideal nucleophile to attack the acyl-enzyme intermediate to release 2-methylbutyric acid (Fig. 2, *D* and *E*). In addition, this H_2O molecule is occupied by one DFP methyl group and simultaneously overlaps with the C–O bond at C8 of lovastatin in Fig. 3*A*, supporting the hypothesis that H_2O is the second nucleophile. We verified this finding using an $H_2{}^{18}O$ isotope-labeling assay, which directly verified H_2O as the second nucleophile. The data showed that the m/z ratio of all characteristic 2-methylbutyric acid fragment ions containing hydroxyl groups increased by 2, compared with a control assay with normal $H_2{}^{16}O$ (Fig. 3*B*). To our knowledge, this is the first direct experimental evidence of the nucleophilic function of H_2O molecules in the currently reported family VIII carboxylesterases.

Based on these analyses, a possible catalytic mechanism of PcEST-mediated lovastatin hydrolysis is proposed (Fig. 4). First, Tyr^{170} (general base), polarized by Lys^{60} (general acid), is bonded to the Ser^{57} hydroxyl to activate the nucleophilic Ser^{57}. Next, lone pairs on the oxygen of Ser^{57} attack the positively charged carbonyl carbon of lovastatin and then form an acyl-enzyme intermediate. Moreover, Tyr^{170} provides a proton for the leaving group to produce monacolin J. Subsequently, H_2O is deprotonated by Tyr^{170} and then nucleophilically attacks the acyl-enzyme intermediate to release 2-methylbutyric acid.

Analyses of reasons for the inactivity of PcEST on simvastatin

Having determined the lovastatin hydrolysis mechanism, we further analyzed why PcEST has no activity toward simvastatin. There are two possibilities: invalid simvastatin ligand binding or steric effects on nucleophilic attack. The first hypothesis was ruled out by ITC experiments, which revealed similar K_D values between PcEST S57A–lovastatin and PcEST–simvastatin. These results indicate similar binding affinity to lovastatin and simvastatin (Fig. S2). Some evidence for the steric effect is found within the PcEST–simvastatin complex structure (Fig. 1*G*). When simvastatin binds the active site, the Ser^{57} hydroxyl is displaced by steric hindrance of the extra methyl in the 2′2-dimethybutyryl side chain. This moves the Ser^{57} hydroxyl away from the carbonyl carbon of simvastatin, thus blocking nucleophilic attack and unfavorable simvastatin catalysis.

The hydrogen-bond network around the catalytic triad is important for enzyme catalytic efficiency

In PcEST, the Trp^{344} in the WGG motif and the Tyr^{127} at the interface of two domains, both forming hydrogen bonds with the catalytic triad and concurrently interacting with statins, might be important for lovastatin hydrolysis efficiency (Fig. 2, *D* and *E*). To verify this hypothesis, we constructed mutants that disrupted the hydrogen-bond network at Trp^{344} and Tyr^{127}. All mutants had dramatically reduced lovastatin hydrolysis, especially W344K and Y127A inactivation mutants (Fig. 2*A*). These results suggest that the hydrogen-bond network around the catalytic triad is important for efficient lovastatin hydrolysis. A possible explanation for W344K inactivation is that Lys^{344} triggers a new possible catalytic triad, Ser^{57}–Lys^{344}–Tyr^{170}, which changes the correct conformation of the Ser^{57} hydroxyl group. In addition, subsequent kinetic analyses of W344F and Y127F showed that Phe replacement caused a dramatic increase in K_m and a decrease in k_{cat} (Table 1), verifying the role of Trp^{344} and Tyr^{127} in substrate binding and in catalysis.

The specific substrate-binding tunnel is also important for the catalytic efficiency of enzymes

In PcEST, R1 (residues 222–248), R2 (residues 127–153), and R3 (residues 290–319) regions around the active site might define the entrance and bottom of the substrate-binding pocket, respectively (Fig. 5). With lovastatin binding, loop 238–245 in R1 increases the entrance size by ~4 Å, likely because of a conformational change to Glu^{241} (Figs. 2*C* and 5). On the opposite side, the Tyr^{127} in the $\pi-\pi$ interaction network forms a new hydrogen bond with Lys^{60} (absent in apo PcEST structure) to stabilize the general acid role of Lys^{60} (Fig. 2, *D* and *E*). These changes imply that the Tyr^{127}-containing R2 region, together with loop 238–245, is a latch for the entrance of the substrate-binding tunnel. Our previously reported Q140L mutant in the R2 helix region, causing a decrease in K_m and an increase in k_{cat} toward lovastatin (9), also indicates the importance of R2 in lovastatin hydrolysis. Further, the Phe^{309} benzene ring at the bottom of the substrate-binding pocket swings away from the hydrophobic core and forms a $\pi-\pi$ interaction with

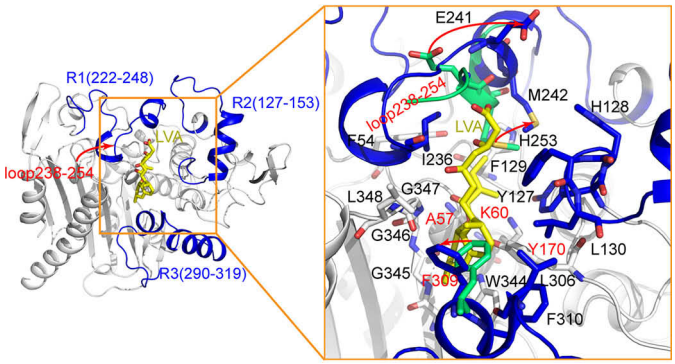

Figure 5. Specific substrate-binding tunnel of PcEST. The R1, R2, and R3 regions, which might define the entrance and bottom of the substrate-binding pocket, are *highlighted* and marked with the corresponding residue numbers. The residues participating in lovastatin (*yellow*) binding are shown as *sticks*. The three significant swings after lovastatin binding (residues Phe^{309}, Glu^{241}, and Met^{242}) in PcEST are marked.

the lovastatin naphthalene ring. Finally, residues Tyr^{170}, Leu^{306}, Phe^{309}, Phe^{310}, Trp^{344}, Gly^{345}, Gly^{346}, Gly^{347}, and Leu^{348} ensure the precise localization of the statin naphthalene ring. Phe^{54}–Ile^{236}–His^{253} and Tyr^{127}–His^{128}–Phe^{129}–Leu^{130}–Met^{242} are separately involved in binding the two acid side chains of lovastatin (Fig. 5). All of these ensure the accurate position of the nucleophilic Ser^{57} hydroxyl group toward lovastatin and initiate the hydrolysis reaction.

Based on these analyses, a possible explanation for Y127A inactivation is that the phenol group absent in the Y127A mutant most likely causes a collapse of the π–π interaction network, which reshapes the PcEST substrate entrance, resulting in its inactivation. However, the structure of Y127A is not yet available to verify this hypothesis. Future studies should investigate the Y127A inactivation mechanism.

Comparison between the lovastatin esterase PcEST and acyltransferase LovD

A Dali-based analysis in the PDB (16) revealed that the top structure matching PcEST is the acyltransferase LovD from *A. terreus* (PDB code 3HLB; Z score = 46.8; root-mean-square deviation = 2.4 Å), which also shares the top sequence identity (~40%) with PcEST among function-identified proteins. LovD mainly catalyzes lovastatin synthesis and concurrently has weak lovastatin hydrolase activity. Ser^{76}–Tyr^{188}–Lys^{79} was reported as its catalytic triad (4). The highly similar primary sequence and three-dimensional core structure between acyltransferase LovD and lovastatin esterase PcEST increases the difficulty of subsequent screening for new efficient lovastatin hydrolases (Figs. S1 and S3). Therefore, the ability to quickly distinguish the acyltransferases and lovastatin esterases will provide notable convenience for screening new specific lovastatin esterases.

In LovD, a relatively wider entrance between R1 and R2 is thought to satisfy the ACP-dependent synthesis (Fig. S3) (4). Moreover, the key WGG motif involving the hydrogen-bond network of PcEST active site is replaced by FGG in all reported LovD homologous acyltransferases (Fig. S1). Additionally, the Phe^{309}–Phe^{310} necessary for lovastatin localization in PcEST is displaced by the Ile^{325}–Tyr^{327} in LovD (Fig. S3), whose conformation changes to generate a new hydrogen-bond network around the general base to regulate the catalytic state of LovD (5). Therefore, these regions can be used as indicators to distinguish acyltransferase and lovastatin esterase.

Structure-guided engineering of PcEST

Our previous work showed that the main problems with PcEST are its poor soluble expression and thermostability (9). The highly flexible regions on protein surfaces sometimes affect the solubility of the proteins and/or reduce their thermostability (17, 18), because they might enhance the entropy during protein unfolding by increasing the numbers of unfolded conformations (19). In the PcEST structure, the long loop in R2 and the antiparallel β-sheet that may participate in the conformation stabilization of R2 helix showed high flexibility with higher structural B factors. Considering that mutations in the R2 region are likely to significantly affect enzyme activity, we first screened for mutation sites in the antiparallel β-sheet. We found that the residues around Asp^{106} are almost hydrophobic residues, involved in the stabilization of the R2 helix. However, the residue Asp^{106}, which is exposed on the surface and is not bonded to any residue, is very flexible and not functionally necessary (Fig. 6*A*). In addition, the Asp^{131} in R2, forming a hydrogen bond with Ser^{161}, might also be involved in R2 stability and then affect catalysis (Fig. 6*B*). Thus, we further engineered Asp^{106} and Asp^{131} using Ala substitution.

Impressively, compared with the slightly reduced catalytic efficiency, the D106A mutant significantly improved the soluble expression level. In addition, the D106A mutant presented a nearly 1 °C increased T_{50}^{10} over the WT PcEST, implying an improved thermostability. Although the catalytic efficiency and soluble expression level of the D131A mutant were almost the same as those of WT PcEST, the T_{50}^{10} was reduced by nearly 3 °C because of mutation, indicating the importance of hydrogen bond for the thermostability of enzymes (Fig. 6*D*). The improved solubility and thermostability of the D106A mutant suggest promising application potential for industrial processes, and on the other hand, the results also demonstrated the feasibility of PcEST structure-guided enzyme engineering. Thus, we will perform saturation mutations on other key sites, such as the R2 loop region, to further improve the properties of PcEST.

Conclusion

The first high-resolution structures of a specific lovastatin esterase were reported in this work. Structure-based biochemical analyses and mutagenesis studies revealed the specific and efficient lovastatin hydrolysis mechanism and the structure–function relationships of PcEST, which will guide subsequent lovastatin esterase screening and engineering. Furthermore, we generated a variant with improved solubility and thermostability, D106A, thus indicating the potential to improve the industrial application of PcEST through structure-guided enzyme engineering.

Materials and methods

Gene cloning and mutagenesis

The PCR-amplified *PcEST* fragment from a *PcEST*–pEASY–Blunt E2 plasmid template (2) was ligated with the pEASY-E1

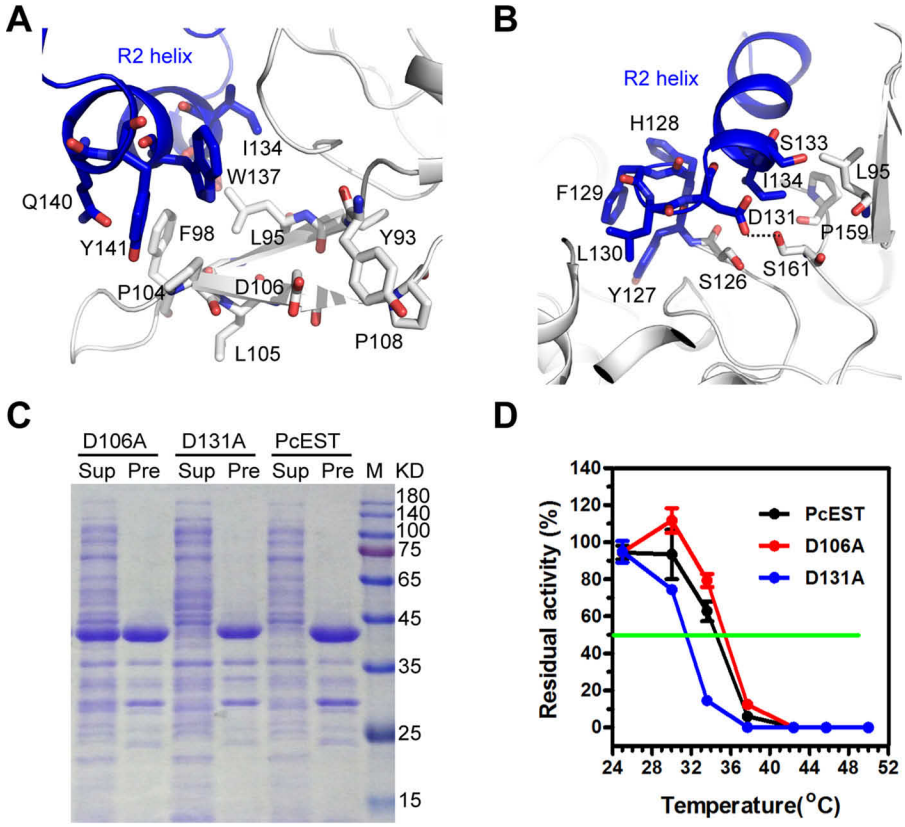

Figure 6. Structure-guided enzyme engineering of PcEST. *A* and *B*, zoomed view of the local environment of Asp[106] (*A*) and Asp131 (*B*) in the PcEST structure. The R2 region of PcEST is colored *blue*. The related residues are shown with *sticks*, and the hydrogen bond is marked by a *black dashed line*. *C* and *D*, expression (*C*) and thermostability (*D*) of PcEST and its mutants. The soluble (*Sup*) and insoluble portions (*Pre*) of PcEST expressed in BL21 (DE3). Thermostability T_{50}^{10} is defined as the temperature where 50% of initial enzyme activity (*green line*) is lost following 10-min heat treatment. Each point represents the means from two independent replicates with standard deviation.

vector (Transgen Biotech) to construct the pEASY–E1–*PcEST* recombinant plasmid, which expresses PcEST with an N-terminal His_6 tag. The *PcEST*–pET28a–smt3 plasmid was constructed using NdeI and XhoI restriction enzymes and expresses PcEST protein with an Ulp1-cleavable N-terminal His_6–smt3 fusion tag. All PcEST mutants used in this study were created using the QuikChange site-directed mutagenesis method, with the *PcEST*–pET28a–smt3 plasmid as the template. All primers are listed in Table S1. Recombinant plasmids were confirmed by DNA sequencing.

Protein expression and purification

All PcEST proteins were expressed in *Escherichia coli* BL21(DE3) (Transgen Biotech) as described previously (2). After induction, the cells were harvested by centrifugation and then sonicated in lysis buffer (20 mM Tris-HCl, pH 8.0, 300 mM NaCl, 10 mM imidazole, 5 mM β-mercaptoethanol, and 10 μg/ml DNase I). The resulting extract was first purified by nickel–nitrilotriacetic acid–agarose resin (Qiagen). His_6-tagged proteins were eluted with buffer containing 20 mM Tris-HCl, pH 8.0, 300 mM NaCl, 250 mM imidazole, and 1 mM β-mercaptoethanol. Next, PcEST–His_6 protein was loaded onto a HiLoad 16/60 Superdex 200 column (GE Healthcare) with buffer A containing 10 mM Tris-HCl, pH 8.0, and 100 mM NaCl. His_6–smt3 fusion PcEST (WT and mutants) proteins were dialyzed and digested with Ulp1 overnight at 4 °C in buffer A and then purified with nickel–nitrilotriacetic acid resin to remove the His_6–smt3 fusion tag. Finally, the target protein was further purified using a Superdex75 10/300 GL column (GE Healthcare) and eluted with buffer A. Protein fractions from each purification step were analyzed by SDS-PAGE. All target proteins were concentrated to 16 mg/ml in buffer A for subsequent protein screening and enzymatic activity.

Crystallization, data collection, and structure determination

Crystallization conditions were screened in 48-well plates at 18 °C by the sitting-drop vapor-diffusion method. A 1:1 protein: reservoir solution ratio and 2-μl total drop size was used for crystallization. Apo PcEST crystals, containing a 17 residue N-terminal flexible extension, were grown at 10 mg/ml in 4 M sodium formate. However, well-ordered enzyme–ligand complex crystals could not be obtained from this procedure. We then removed the flexible extension using the vector *PcEST*–pET28a–smt3 in subsequent crystallization experiments.

For the enzyme–ligand complex, 10 mg/ml PcEST (WT or the inactivated mutant S57A) was incubated with 3.5 mM ligand, monacolin J, simvastatin, or lovastatin at 4 °C for 2 h. Diffraction-quality crystals of S57A-lovastatin were obtained in 2–3 days when grown in 200 mM calcium acetate, 100 mM Tris-HCl, pH 7.0, and 20% (w/v) PEG 3000. The PcEST–monacolin J and PcEST–simvastatin crystals were grown in crystallization buffer (200 mM calcium acetate, 100 mM sodium cacodylate

trihydrate, pH 6.5, and 18% (w/v) PEG 8000) for 2 days. The crystals were harvested and cryoprotected in crystallization solution containing 16% glycerol or 20% (v/v) PEG 400 and flash-cooled in liquid nitrogen.

The diffraction data were collected at the National Center for Protein Sciences Shanghai (Shanghai, China), using Beamline BL19U1 (apo PcEST), or the Beijing Synchrotron Radiation Facility (Beijing, China) for PcEST–monacolin J, PcEST–simvastatin, and S57A–lovastatin complex structures. The data were processed using HKL3000 or HKL2000 software (20, 21). The apo PcEST structure was solved with molecular replacement using Phaser (22) and coordinates of LovD6 from *A. terreus* as a search model (PDB code 4LCL). LovD6 shares 36% identity over 147 residues with PcEST. Two protein molecules were found in the asymmetric unit. The phases for subsequent enzyme–ligand complex structures were also obtained by molecular replacement using apo PcEST as the search model. An additional electron density appeared at the proposed substrate-binding pocket. The structures were refined using Refmac or Phenix.refine software and were manually corrected in Coot in iterative rounds (23–25). Final model quality was checked using MolProbity (26). A data collection and final refinement statistics summary is found in Table S2. PyMOL was used to prepare all structural figures (27).

Enzymatic characterization of PcEST and its mutants in vitro

The general reaction system consisted of 0.05 μM WT PcEST protein or 5 μM mutants, 400 μM lovastatin and 50 mM Tris-HCl pH 8.0 buffer. After incubation at 30 °C for 30 min, the hydrolysis reaction was quenched by adding an equal volume of 100% anhydrous methanol. The HPLC detection method was described previously (2).

For the determination of thermostability, the purified proteins (0.5 mg/ml) were preincubated at temperatures from 25 to 50 °C for 10 min using the temperature gradient function on PCR (Bio-Rad T100*) and then quickly cooled on ice. The lovastatin hydrolysis reaction was performed as described above.

We assessed kinetic parameters (K_m and k_{cat}) of PcEST, Y127F, W344F, D106A, and D131A mutants at 30 °C. First, enzyme and lovastatin substrate concentrations and reaction times were optimized. The final lovastatin concentration varied from 3 to 200 μM for PcEST (0.01 μM), D106A (0.005 μM), and D131A (0.01 μM); 25–700 μM for Y127F (0.5 μM); and 15–700 μM for W344F (3 μM) in 50 mM Tris-HCl pH 8.0 buffer. At least two independent experiments were performed for each reaction time point. The kinetic curve was drawn by fitting the initial rate data into the Michaelis–Menten equation using GraphPad Prism version 5.0.0 software.

Analysis of soluble expression levels of PcEST and its mutants

The analysis strategy for the soluble expression levels of PcEST and its mutants was described previously (9). The expression plasmids lacking fusion tags, pET22–D106A and pET22–D131A, were constructed using the QuikChange site-directed mutagenesis method with pET22–PcEST as the template (9). Plasmids were transformed into BL21 (DE3) cells and induced with 0.2 mM isopropyl β-D-thiogalactopyranoside at 25 °C for 16 h. The harvested cells were lysed by sonication. After centrifugation at 4 °C, the supernatant and resuspended precipitate fractions were analyzed by SDS-PAGE.

Isothermal titration calorimetry assays

ITC experiments were performed at 25 °C with a MicroCal iTC200 (GE Healthcare) using 60 μM enzyme in the sample cell and 1 mM ligand in the syringe. Thirteen injections (3 μl each) were used. The dilution heat for each ligand was measured in a separate titration experiment by titrating ligand into buffer. Consecutive injections were separated by at least 2 min. The ITC data were analyzed with one sites model using Origin 8.0 software (OriginLab).

$H_2{}^{18}O$ isotope labeling assays

The $H_2{}^{18}O$ used in the reaction buffer was purchased from Macklin (CAS: 14314-42-2). To obtain sufficient 2-methylbutyric acid for GC-MS detection, 10 mM lovastatin was completely hydrolyzed by 0.05 μM PcEST at 30 °C and 110 rpm overnight. The reaction mixture (1 μl) was diluted by 100% anhydrous methanol and analyzed by GC-MS using an Agilent 7890A-5975C system equipped with a HP-5 column (30 m × 250 μm × 0.25 μm). Helium (constant flow 1 ml/min) was used as the carrier gas. The injector temperature was 250 °C, and the following temperature program was applied: initial temperature 40 °C for 0 min, 10 °C/min to 250 °C in the ramp step, and maintained at 250 °C for 10 min. A 2-methylbutyric acid standard was used as a control.

Author contributions—Y. L. data curation; Y. L. and X. L. formal analysis; Y. L. and X. L. funding acquisition; Y. L. and X. L. validation; Y. L. investigation; Y. L. visualization; Y. L. methodology; Y. L. writing-original draft; Y. L. and X. L. project administration; X. L. conceptualization; X. L. supervision; X. L. writing-review and editing.

Acknowledgments—We thank Dr. Zengqiang Gao and the staffs of the 3W1B Beamline at the Beijing Synchrotron Radiation Facility and the staffs of the BL19U1 Beamline at National Center for Protein Sciences Shanghai for assistance during data collection. Cong Wang from the Qingdao Institute of Bioenergy and Bioprocess Technology of the Chinese Academy of Sciences provided technical support for MS.

References

1. Hoffman, W. F., Alberts, A. W., Anderson, P. S., Chen, J. S., Smith, R. L., and Willard, A. K. (1986) 3-Hydroxy-3-methylglutaryl-coenzyme A reductase inhibitors: 4. Side chain ester derivatives of mevinolin. *J. Med. Chem.* **29,** 849–852 CrossRef Medline
2. Huang, X., Liang, Y., Yang, Y., and Lu, X. (2017) Single-step production of the simvastatin precursor monacolin J by engineering of an industrial strain of *Aspergillus terreus*. *Metab. Eng.* **42,** 109–114 CrossRef Medline
3. Xie, X., and Tang, Y. (2007) Efficient synthesis of simvastatin by use of whole-cell biocatalysis. *Appl. Environ. Microb.* **73,** 2054–2060 CrossRef Medline
4. Gao, X., Xie, X., Pashkov, I., Sawaya, M. R., Laidman, J., Zhang, W., Cacho, R., Yeates, T. O., and Tang, Y. (2009) Directed evolution and structural characterization of a simvastatin synthase. *Chem. Biol.* **16,** 1064–1074 CrossRef Medline
5. Jiménez-Osés, G., Osuna, S., Gao, X., Sawaya, M. R., Gilson, L., Collier, S. J., Huisman, G. W., Yeates, T. O., Tang, Y., and Houk, K. N. (2014) The role of distant mutations and allosteric regulation on LovD active site dynamics. *Nat. Chem. Biol.* **10,** 431–436 CrossRef Medline

6. Schimmel, T. G., Borneman, W. S., and Conder, M. J. (1997) Purification and Characterization of a lovastatin esterase from *Clonostachys compactiuscula*. *Appl. Environ. Microbiol.* **63,** 1307–1311 Medline
7. Chen, L.-C., Lai, Y.-K., Wu, S.-C., Lin, C.-C., and Guo, J.-H. (2006) Production by *Clonostachys compactiuscula* of a lovastatin esterase that converts lovastatin to monacolin J. *Enzyme Microb. Technol.* **39,** 1051–1059 CrossRef
8. Morgan, B., Burk, M., Levin, M., Zhu, Z., Chaplin, J., Kustedjo, K., Huang, Z., and Greenberg, W. (2004) Methods for making simvastatin and intermediates. U. S. Patent 20080182303, July 31, 2008
9. Liang, B., Huang, X., Teng, Y., Liang, Y., Yang, Y., Zheng, L., and Lu, X. (2018) Enhanced single-step bioproduction of the simvastatin precursor monacolin J in an industrial strain of *Aspergillus terreus* by employing the evolved lovastatin hydrolase. *Biotechnol. J.* **13,** e1800094 Medline
10. Xie, X., Watanabe, K., Wojcicki, W. A., Wang, C. C., and Tang, Y. (2006) Biosynthesis of lovastatin analogs with a broadly specific acyltransferase. *Chem. Biol.* **13,** 1161–1169 CrossRef Medline
11. Wagner, U. G., Petersen, E. I., Schwab, H., and Kratky, C. (2002) EstB from Burkholderia gladioli: a novel esterase with a β-lactamase fold reveals steric factors to discriminate between esterolytic and β-lactam cleaving activity. *Protein Sci.* **11,** 467–478 Medline
12. Arpigny, J. L., and Jaeger, K. E. (1999) Bacterial lipolytic enzymes: classification and properties. *Biochem. J.* **343,** 177–183 CrossRef Medline
13. Joris, B., Ghuysen, J. M., Dive, G., Renard, A., Dideberg, O., Charlier, P., Frère, J. M., Kelly, J. A., Boyington, J. C., Moews, P. C., and Knox, J. R. (1988) The active-site-serine penicillin-recognizing enzymes as members of the *Streptomyces* R61 Dd-peptidase family. *Biochem. J.* **250,** 313–324 CrossRef Medline
14. Cha, S. S., and An, Y. J. (2016) Crystal structure of EstSRT1, a family VIII carboxylesterase displaying hydrolytic activity toward oxyimino cephalosporins. *Biochem. Biophys. Res. Commun.* **478,** 818–824 CrossRef Medline
15. Cha, S. S., An, Y. J., Jeong, C. S., Kim, M. K., Jeon, J. H., Lee, C. M., Lee, H. S., Kang, S. G., and Lee, J. H. (2013) Structural basis for the β-lactamase activity of EstU1, a family VIII carboxylesterase. *Proteins* **81,** 2045–2051 CrossRef Medline
16. Holm, L., and Sander, C. (1995) Dali: a network tool for protein structure comparison. *Trends Biochem. Sci.* **20,** 478–480 CrossRef Medline
17. Fang, Z., Zhou, P., Chang, F., Yin, Q., Fang, W., Yuan, J., Zhang, X., and Xiao, Y. (2014) Structure-based rational design to enhance the solubility and thermostability of a bacterial laccase Lac15. *PLoS One* **9,** e102423 CrossRef Medline
18. Yainoy, S., Phuadraksa, T., Wichit, S., Sompoppokakul, M., Songtawee, N., Prachayasittikul, V., and Isarankura-Na-Ayudhya, C. (2019) Production and characterization of recombinant wild type uricase from indonesian coelacanth (*L. menadoensis*) and improvement of its thermostability by *in silico* rational design and disulphide bridges engineering. *Int. J. Mol. Sci.* **20,** E1269 Medline
19. Malakauskas, S. M., and Mayo, S. L. (1998) Design, structure and stability of a hyperthermophilic protein variant. *Nat. Struct. Biol.* **5,** 470–475 CrossRef Medline
20. Minor, W., Cymborowski, M., Otwinowski, Z., and Chruszcz, M. (2006) HKL-3000: the integration of data reduction and structure solution: from diffraction images to an initial model in minutes. *Acta Crystallogr. D Biol. Crystallogr* **62,** 859–866 CrossRef Medline
21. Otwinowski, Z., and Minor, W. (1997) Processing of X-ray diffraction data collected in oscillation mode. *Methods Enzymol.* **276,** 307–326 CrossRef Medline
22. McCoy, A. J., Grosse-Kunstleve, R. W., Adams, P. D., Winn, M. D., Storoni, L. C., and Read, R. J. (2007) Phaser crystallographic software. *J. Appl. Crystallogr.* **40,** 658–674 CrossRef Medline
23. Murshudov, G. N., Vagin, A. A., and Dodson, E. J. (1997) Refinement of macromolecular structures by the maximum-likelihood method. *Acta Crystallogr. D Biol. Crystallogr.* **53,** 240–255 CrossRef Medline
24. Adams, P. D., Afonine, P. V., Bunkóczi, G., Chen, V. B., Davis, I. W., Echols, N., Headd, J. J., Hung, L. W., Kapral, G. J., Grosse-Kunstleve, R. W., McCoy, A. J., Moriarty, N. W., Oeffner, R., Read, R. J., Richardson, D. C., *et al.* (2010) PHENIX: a comprehensive Python-based system for macromolecular structure solution. *Acta Crystallogr. D Biol. Crystallogr.* **66,** 213–221 CrossRef Medline
25. Emsley, P., Lohkamp, B., Scott, W. G., and Cowtan, K. (2010) Features and development of Coot. *Acta Crystallogr. D Biol. Crystallogr.* **66,** 486–501 CrossRef Medline
26. Chen, V. B., Arendall, W. B., 3rd, Headd, J. J., Keedy, D. A., Immormino, R. M., Kapral, G. J., Murray, L. W., Richardson, J. S., and Richardson, D. C. (2010) MolProbity: all-atom structure validation for macromolecular crystallography. *Acta Crystallogr. D Biol. Crystallogr.* **66,** 12–21 CrossRef Medline
27. DeLano, W. L. (2015) *The PyMOL Molecular Graphics System*, version 1.8, Schroedinger, LLC, New York